

# Model Predictive Control of Structures under Earthquakes using Acceleration Feedback

Gang Mei<sup>1</sup>; Ahsan Kareem<sup>2</sup>; and Jeffrey C. Kantor<sup>3</sup>

**Abstract:** This paper presents a general formulation of the model predictive control (MPC) scheme with special reference to acceleration feedback in structural control under earthquakes. The MPC scheme is based on a prediction model of the system response to obtain the control action by minimizing an objective function. Optimization objectives include minimization of the difference between the predicted and desired response trajectories, and of the control effort subject to certain constraints. The effectiveness of MPC has been demonstrated to be equivalent to the optimal control. In this study, the prediction model is formulated using a feedback loop containing acceleration measurements from various locations in the structure. The state observer utilizes the Kalman-Bucy filter to estimate the states of the system from the acceleration feedback. Examples of single-story and three-story buildings equipped with control devices are used to demonstrate the effectiveness of the MPC scheme based on acceleration feedback. Both buildings are analyzed using an active tendon control device and an active mass damper (AMD). A two-story building with an AMD is used to experimentally validate the numerical control scheme. The results demonstrate the effectiveness of the MPC scheme using acceleration feedback. The acceleration feedback framework developed in this paper should serve as a building block for future extensions of MPC in capturing and benefiting from the attractive features of MPC, i.e., computational expediency, real-time applications, intrinsic compensation for time delays, and treatment of constraints, for implementation in civil structures.

**DOI:** 10.1061/(ASCE)0733-9399(2002)128:5(574)

**CE Database keywords:** Earthquakes; Predictive control; Models; Acceleration; Structural control.

## Introduction

Structural control devices are becoming increasingly popular for improving the performance of a wide range of structures, e.g., bridges, tall buildings, and offshore structures (Soong 1990; Housner et al. 1997; Soong and Dargush 1997; Kareem et al. 1999). These control devices can be categorized as passive or active. The passive devices function without an external power source. To enhance the performance of damping devices, external control action is introduced in active systems, which requires design and implementation of a control law. The most commonly used control scheme in these devices is the linear quadratic regulator (Soong 1990; Housner et al. 1997). Other schemes like the  $H_2$  and  $H_\infty$  have been employed in civil engineering control applications (Doyle et al. 1989; Suhardjo et al. 1992; Spencer et al. 1994; Suhardjo and Kareem 1997). Dyke et al. (1996) studied digital implementation of  $H_2$ -based control schemes. The sliding mode control scheme was introduced by Utkin (1977) and Slotine

(1984), and Yang et al. (1994) experimentally verified its effectiveness for buildings with active tendon devices. Rodellar et al. (1987) and Lopez-Almansa et al. (1994a,b) applied predictive control schemes in civil engineering studies. However, in their approach the objective function was expressed in term of the predicted trajectory and control force for one time step only. The control force is related to the state of the system by a constant gain matrix. Since the desirable reference trajectory is zero, it can be easily shown that the optimal control force is zero, which is not a viable control design. This problem does not exist in the model predictive control (MPC) scheme, which is the focus of this study, since the objective function is expressed in terms of the predicted trajectory and control force over the prediction horizon.

The MPC scheme has been commonly used for control in the chemical, automotive, and aerospace industries (Ricker 1990; Morari et al. 1994; Qin and Badgwell 1996; Camacho and Bordons 1999). Recently it has been applied to the control of civil engineering structures by Mei et al. (1998). The MPC scheme is based on explicit use of a prediction model of the system response to obtain the control action by minimizing an objective function. Optimization objectives include minimization of the difference between the predicted and reference response and minimization of the control effort subjected to certain constraints. Model predictive control uses a linear structural model and a quadratic objective function. In the absence of inequality constraints on the system, MPC is equivalent to linear quadratic optimal control. In the case of long prediction horizons, the performance of MPC approaches that of the  $H_2$  control scheme. The MPC scheme also offers advantages in computational expediency, real-time applications, intrinsic compensation for time delays, and treatment of constraints (Morari and Lee 1991; Mei et al. 1998, 2000, 2001).

<sup>1</sup>Research Assistant, NatHaz Modeling Laboratory, Dept. of Civil Engineering and Geological Sciences, Univ. of Notre Dame, Notre Dame, IN 46556.

<sup>2</sup>Professor and Chair, Dept. of Civil Engineering and Geological Sciences, Univ. of Notre Dame, Notre Dame, IN 46556.

<sup>3</sup>Vice-President and Associate Provost, Professor, Dept. of Chemical Engineering, Univ. of Notre Dame, Notre Dame, IN 46556.

Note. Associate Editor: James L. Beck. Discussion open until October 1, 2002. Separate discussions must be submitted for individual papers. To extend the closing date by one month, a written request must be filed with the ASCE Managing Editor. The manuscript for this paper was submitted for review and possible publication on October 18, 2000; approved on July 31, 2001. This paper is part of the *Journal of Engineering Mechanics*, Vol. 128, No. 5, May 1, 2002. ©ASCE, ISSN 0733-9399/2002/5-574-585/\$8.00+\$0.50 per page.

Most of the above control strategies utilize the displacement and/or velocity response measurements of the structure. However, directly measuring these response components can be quite difficult because the displacement and velocity are not absolute measurements, i.e., they need a fixed reference frame. In addition, during an earthquake, a structure's foundation is moving with the ground, and thus does not provide a convenient fixed reference coordinate system. Therefore, control algorithms based on such measurements are impracticable for full-scale implementation; thus the acceleration response feedback becomes an attractive option. Measuring the earthquake-induced acceleration response at different locations in the structure by means of accelerometers is relatively convenient (e.g., Dyke et al. 1996).

This paper employs the MPC scheme to reduce the structural response of linear structures under earthquakes using acceleration response feedback. The Kalman-Bucy filter in the state observer is used to estimate the states of the system from the acceleration output feedback. Four examples are used to demonstrate the acceleration feedback methodology. The first two examples analyze two buildings using active tendon devices. In the second set of examples the same buildings are analyzed using active mass dampers (AMDs). The first building in each case is a single-degree-of-freedom (SDOF) system. The second example involves a three-story building. For the SDOF system, the results of the acceleration feedback analysis are compared to those obtained from analysis of the system using state feedback. In addition to the above analysis, in the three-story building example, the influence of accelerometer locations on the effectiveness of the controller was also examined. Finally, a small-scale experiment was conducted at the NatHaz Modeling Laboratory, University of Notre Dame. The MPC scheme using acceleration feedback was digitally implemented using a two-story building with an AMD.

## Problem Formulation

A linear structure is modeled as an  $n$ -degree-of-freedom system

$$\mathbf{M}\ddot{\mathbf{x}} + \mathbf{C}\dot{\mathbf{x}} + \mathbf{K}\mathbf{x} = \mathbf{F} - \mathbf{M}\mathbf{I}\ddot{\mathbf{x}}_g \quad (1)$$

where  $\mathbf{M}$ ,  $\mathbf{C}$ , and  $\mathbf{K}$ =mass, damping, and stiffness matrices, respectively;  $\mathbf{x}$ ,  $\dot{\mathbf{x}}$ , and  $\ddot{\mathbf{x}}$ = $n \times 1$  displacement, velocity, and acceleration vectors relative to the ground;  $\mathbf{I}=n \times 1$  identity vector;  $\ddot{\mathbf{x}}_g$ =ground acceleration; and  $\mathbf{F}=\mathbf{L}u=n \times 1$  control force vector generated by placing the actuator on different floors.  $\mathbf{L}=n \times m$  matrix with elements equal to zero or 1 depending on the placement of the actuator on different floors.  $u=m \times 1$  control force vector. Rewriting the equations of motion in the state space format

$$\dot{\mathbf{x}} = \begin{bmatrix} \dot{\mathbf{x}} \\ \ddot{\mathbf{x}} \end{bmatrix} = \begin{bmatrix} 0 & \mathbf{I} \\ -\mathbf{M}^{-1}\mathbf{K} & -\mathbf{M}^{-1}\mathbf{C} \end{bmatrix} \begin{bmatrix} \mathbf{x} \\ \dot{\mathbf{x}} \end{bmatrix} + \begin{bmatrix} 0 \\ \mathbf{M}^{-1}\mathbf{L} \end{bmatrix} u + \begin{bmatrix} 0 \\ -\mathbf{I} \end{bmatrix} \ddot{\mathbf{x}}_g = \mathbf{A}\mathbf{x} + \mathbf{B}u + \mathbf{G}\ddot{\mathbf{x}}_g \quad (2)$$

where  $\mathbf{G}$ =vector representing the seismic load distribution.

For digital implementation of control, Eq. (2) is expressed in a discrete time format:

$$\mathbf{x}((k+1)\Delta t) = \Phi\mathbf{x}(k\Delta t) + \Gamma_u u(k\Delta t) + \Gamma_d \ddot{\mathbf{x}}_g(k\Delta t) \quad (3)$$

where  $\Phi = e^{\mathbf{A}\Delta t} = 2n \times 2n$  matrix;  $\Gamma_u = \mathbf{P}_1\mathbf{B}$  and  $\Gamma_d = \mathbf{P}_1\mathbf{G} = 2n \times m$  matrices for which  $\mathbf{P}_1 = \int_0^{\Delta t} e^{\mathbf{A}\tau} d\tau = 2n \times 2n$  matrix; and  $\Delta t$ =sampling time. This building model is then combined with the output values obtained in the following section to establish an overall system model.

The overall system model can be expressed as

$$\begin{aligned} \mathbf{x}(k+1) &= \Phi(k)\mathbf{x}(k) + \Gamma_u(k)u(k) + \Gamma_d(k)\ddot{\mathbf{x}}_g(k) \\ \mathbf{z}(k) &= \mathbf{C}_z\mathbf{x}(k) + \mathbf{D}_z u(k) \end{aligned} \quad (4)$$

$$\mathbf{y}(k) = \mathbf{C}\mathbf{x}(k) + \mathbf{D}_u u(k) + \mathbf{D}_d \ddot{\mathbf{x}}_g + v$$

in which  $\mathbf{z}(k)$ =controlled output vector that will be used in the objective function;  $\mathbf{y}(k)$ =measured output;  $v$ =measurement noise; in this paper  $\mathbf{C}_z = \mathbf{I}$  and  $\mathbf{D}_z = 0$ , and

$$\mathbf{C} = [-\mathbf{M}^{-1}\mathbf{K} - \mathbf{M}^{-1}\mathbf{C}] \quad (5)$$

$$\mathbf{D}_u = -\mathbf{M}^{-1}\mathbf{L}, \quad \mathbf{D}_d = 0 \quad (6)$$

## Acceleration Feedback and State Estimator

As stated earlier, acceleration is more straightforward and convenient to measure than the displacement and velocity response, which define the states of the system. The main assumption involved in using the Kalman filter in the MPC scheme is that the input and output disturbances are random with zero mean values (Ricker 1990). According to the separation principle (Kailath 1980), the control and estimation problems can be considered separately. Therefore, the estimator gain can be obtained independent of the feedback gain. The full state vector  $\mathbf{x}(k)$  is reconstructed using an observer to obtain the estimate of the state vector  $\hat{\mathbf{x}}(k)$ . It can be constructed in the following manner:

$$\hat{\mathbf{x}}(k+1) = \Phi\hat{\mathbf{x}}(k) + \Gamma_u u(k) + \Gamma_e(\mathbf{y}(k) - \hat{\mathbf{y}}(k)) \quad (7)$$

where  $\hat{\mathbf{y}}(k) = \mathbf{C}\hat{\mathbf{x}}(k) + \mathbf{D}_u u(k)$  and  $\Gamma_e$  is related to the Kalman-Bucy filter

$$\Gamma_e = \mathbf{P}\mathbf{C}^T(\mathbf{C}\mathbf{P}\mathbf{C}^T + \mathbf{V})^{-1} \quad (8)$$

where  $\mathbf{P}$  is the unique, symmetric, positive definite solution of the Riccati equation

$$\mathbf{P} = \Phi[\mathbf{P} - \mathbf{P}\mathbf{C}^T(\mathbf{C}\mathbf{P}\mathbf{C}^T + \mathbf{V})^{-1}\mathbf{C}\mathbf{P}]\Phi + \Gamma_d \mathbf{W} \Gamma_d^T \quad (9)$$

where  $\mathbf{W} = E[\ddot{\mathbf{x}}_g \ddot{\mathbf{x}}_g^T]$ ;  $\mathbf{V} = E[vv^T]$ ;  $\mathbf{W} = \mathbf{W}^T$  when  $\mathbf{W} > 0$ ; and  $\mathbf{V} = \mathbf{V}^T$  when  $\mathbf{V} > 0$ . It is assumed here that  $\ddot{\mathbf{x}}_g$  and  $v$  are uncorrelated with each other, i.e.,  $E[\ddot{\mathbf{x}}_g v^T] = 0$ .

## Model Predictive Control

The MPC scheme is based on explicit use of a prediction model of the system response to obtain the control action by minimizing an objective function. The optimization objective is posed as a trade-off function for minimization of the difference between the predicted and desired response and the control effort subject to certain constraints. The MPC scheme offers a very general framework for posing the control problem in the time domain, which integrates features involving optimal control, stochastic control, control of processes with time delays, multivariable control, and future references. The concept is not limited to a particular system description, but the computation and implementation depend on the model representation, e.g., state space, transfer matrix, etc. Inclusion of constraints is conceptually simple and they can be systematically included during the design and implementation of the controller.

The basic principle of the MPC scheme is illustrated in Fig. 1(a). First, a reference trajectory  $\mathbf{y}_r(k)$  is specified. This trajectory represents the desired target trajectory for the system response. Second, an appropriate prediction model is used to predict the

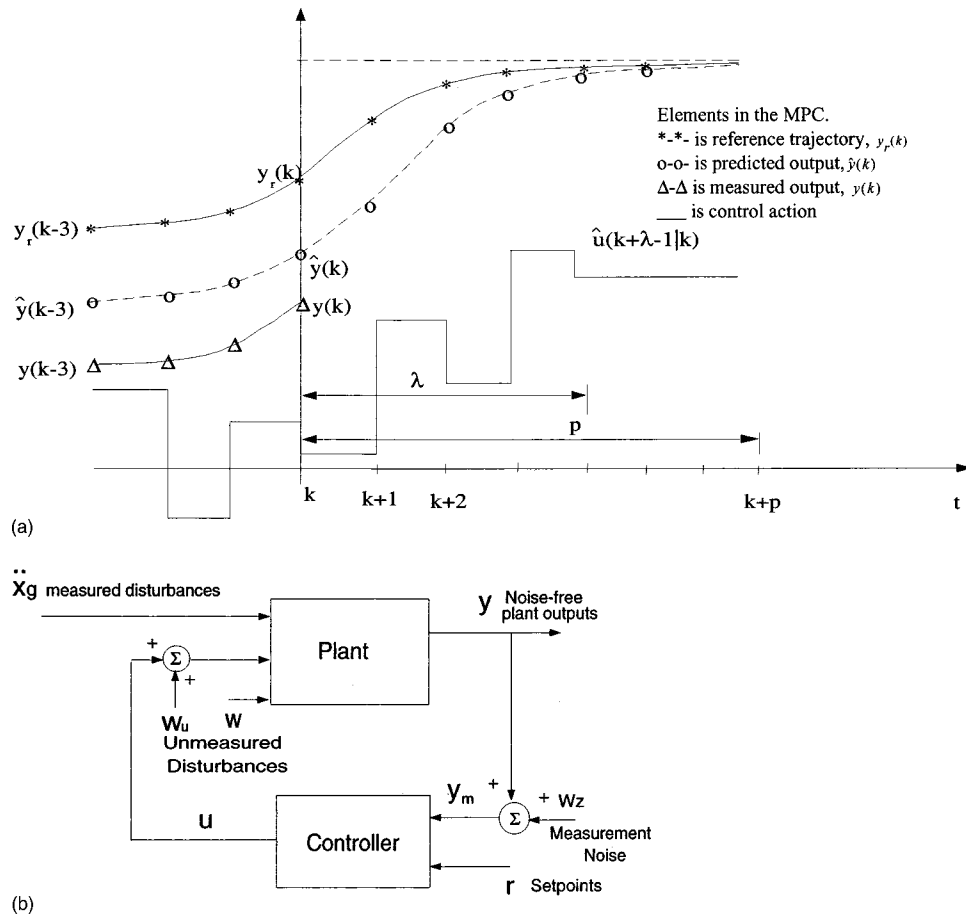


Fig. 1. (a) Basic model predictive control scheme; (b) control diagram

future system responses  $\hat{y}(k)$ . The prediction is made over a pre-established extended time horizon, using the current time as the prediction origin. For a discrete time model, this means predicting  $\hat{y}(k+1)$ ,  $\hat{y}(k+2)$ , ...,  $\hat{y}(k+i)$  for  $i$  sample times in the future. This prediction is based both on actual past control inputs  $u(k)$ ,  $u(k-1)$ , ...,  $u(k-j)$  and on the sequence of future control efforts that are needed to satisfy a prescribed optimization objective determined using the prediction model. Such an optimization objective includes minimization of the difference between the predicted and target responses and of the control effort needed to reach this objective subject to certain constraints, such as limits on the magnitude of the control force. Third, the control signals that were determined using the prediction model are then applied to the structure, and the actual system output  $y(k)$  is found. Finally, the actual measurement  $y(k)$  is compared to the model prediction  $\hat{y}(k)$  and the prediction error  $[\hat{e}(k) = y(k) - \hat{y}(k)]$  is utilized to update future predictions.

In general model predictive control, the discrete time state space equations of the system are expressed as

$$\begin{aligned} \mathbf{x}(k+1) &= \Phi \mathbf{x}(k) + \Gamma U(k) \\ \mathbf{y}(k) &= C \mathbf{x}(k) + D U(k) \end{aligned} \quad (10)$$

where

$$U(k) = [u^T(k) \quad \ddot{x}_g^T(k) \quad v(k)]^T \quad (11)$$

The unmeasured system disturbance noise  $w(k)$ , control input noise  $w_u(k)$ , and output measurement noise  $w_z(k)$  may be combined as a single noise variable  $v$ , and  $D = [D_u D_d I]$ . Additional

assumptions can be made including setting the future noise to zero and using the system state space model to estimate the future state of the plant. The prediction model can be expressed as

$$\begin{aligned} \hat{\mathbf{x}}(k+1|k) &= \Phi \hat{\mathbf{x}}(k|k-1) + \Gamma_u \hat{u}(k|k-1) + \Gamma_e \hat{e}(k|k) \\ \hat{\mathbf{z}}(k|k-1) &= C_z \hat{\mathbf{x}}(k|k-1) \\ \hat{y}(k|k-1) &= C \hat{\mathbf{x}}(k|k-1) + D_u \hat{u}(k|k-1) \end{aligned} \quad (12)$$

where  $\hat{\mathbf{x}}(k+1|k)$  estimates the state at the future sampling period  $k+1$  based on the information available at  $k$ ;  $\hat{y}(k|k-1)$  estimates the plant output at period  $k$  based on the information available at period  $k-1$ ;  $\Gamma_e$  = Kalman-Bucy estimator gain matrix; and  $\hat{e}(k|k) =$  estimated error:  $\hat{e}(k|k) = y(k) - \hat{y}(k|k-1)$ .

Using Eq. (10), the process output predicted at the  $k$ th time step and at subsequent time steps  $k+j$ ,  $j=1, \dots, p$ , can be expressed as a function of the current state vector  $\mathbf{x}(k)$  and the control vector  $\mathbf{u}(k) = [\hat{u}^T(k|k) \cdots \hat{u}^T(k+\lambda-1|k)]^T$  as follows:

$$\Psi(k) = H \mathbf{u}(k) + Y_z \hat{\mathbf{x}}(k|k-1) + Y_e \hat{e}(k|k) \quad (13)$$

and  $\Psi(k) = [\hat{\mathbf{z}}^T(k+1|k) \cdots \hat{\mathbf{z}}^T(k+p|k)]^T$ , where  $p$  = prediction horizon; and  $\lambda$  = control horizon. The reference output can be written as  $\Psi_r(k) = [\mathbf{z}_r^T(k+1|k) \cdots \mathbf{z}_r^T(k+p|k)]^T$ .

Therefore, the objective function is given by

$$J = \frac{1}{2} [\Psi(k) - \Psi_r(k)]^T \bar{Q} [\Psi(k) - \Psi_r(k)] + \frac{1}{2} \mathbf{u}^T(k) \bar{R} \mathbf{u}(k) \quad (14)$$

By minimizing  $J$ , the optimal predictive control force is given by

$$\mathbf{u} = [H^T \bar{Q} H + \bar{R}]^{-1} H^T \bar{Q} [Y_z \hat{\mathbf{x}}(k|k-1) + Y_e \hat{e}(k|k)] \quad (15)$$

in which

$$H = \begin{bmatrix} H_1 & 0 & \cdots & 0 \\ \cdots & \cdots & \cdots & \cdots \\ H_\lambda & H_{\lambda-1} & \cdots & H_1 \\ H_{\lambda+1} & H_\lambda & \cdots & H_1 + H_2 \\ \cdots & \cdots & \cdots & \cdots \\ H_p & H_{p-1} & \cdots & H_1 + \cdots + H_{p-\lambda} \end{bmatrix} \quad (16)$$

$$H_k = C_z \Phi^{k-1} \Gamma_u \quad (16)$$

$$Y_z = [(C_z \Phi)^T (C_z \Phi^2)^T \cdots (C_z \Phi^p)^T]^T \quad (17)$$

$$Y_e = \left[ (C_z \Gamma_e)^T (C_z (I + \Phi) \Gamma_e)^T \cdots \left( C_z \sum_{k=1}^p (\Phi^{k-1}) \Gamma_e \right)^T \right]^T \quad (18)$$

$$\bar{Q} = \begin{bmatrix} Q & \cdots & 0 \\ \cdots & \cdots & \cdots \\ 0 & \cdots & Q \end{bmatrix}, \quad \bar{R} = \begin{bmatrix} R & \cdots & 0 \\ \cdots & \cdots & \cdots \\ 0 & \cdots & R \end{bmatrix} \quad (19)$$

The control variable taken at each time step is  $u(k) = \hat{u}(k|k)$ . It can be expressed as

$$u(k) = K_1 \hat{\mathbf{x}}(k|k-1) + K_2 e(k|k) \quad (20)$$

where  $K_1$  = first row of  $[H^T \bar{Q} H + \bar{R}]^{-1} H^T \bar{Q} Y_z$ ; and  $K_2$  = first row of  $[H^T \bar{Q} H + \bar{R}]^{-1} H^T \bar{Q} Y_e$ .

The system and observer can then be expressed in state space equations as follows

$$\begin{bmatrix} \mathbf{x}(k+1) \\ \hat{\mathbf{x}}(k+1|k) \end{bmatrix} = \begin{bmatrix} \Phi + \Gamma_u K_2 C & \Gamma_u K_1 - \Gamma_u K_2 C \\ (\Gamma_u K_2 + \Gamma_e) C & \Phi + \Gamma_u K_1 - (\Gamma_u K_2 + \Gamma_e) C \end{bmatrix} \times \begin{bmatrix} \mathbf{x}(k) \\ \hat{\mathbf{x}}(k|k-1) \end{bmatrix} + \begin{bmatrix} \Gamma_u K_2 D_d + \Gamma_d \\ (\Gamma_u K_2 + \Gamma_e) D_d \end{bmatrix} \ddot{x}_g(k) \quad (21)$$

$$\mathbf{y}(k) = [C + D_u K_2 C D_u K_1 - D_u K_2 C] \begin{bmatrix} \mathbf{x}(k) \\ \hat{\mathbf{x}}(k|k-1) \end{bmatrix} + [D_d + D_u K_2 D_d] \ddot{x}_g(k) \quad (22)$$

The stability of the MPC scheme has been discussed in detail by Garcia and Morari (1982), Kwon and Byun (1989), and Zafiriou (1991). It was shown that there exists a finite horizon over which the closed-loop systems are always asymptotically stable. For the stable system, the eigenvalues of the matrix  $\Phi + \Gamma_u K_2 C$  are inside the unit circle.

The MPC formulation presented in the preceding section is utilized in the following examples to demonstrate its applications to building structures.

## Numerical Examples

Four numerical examples are presented below to demonstrate the acceleration feedback scheme presented earlier. This scheme is first applied to two buildings, each utilizing an active tendon device. It is then applied to the same two buildings each equipped with an AMD. The 1940 El Centro earthquake record was scaled to 0.25 of its maximum intensity for dynamic similarity and used in this study as the input ground motion.

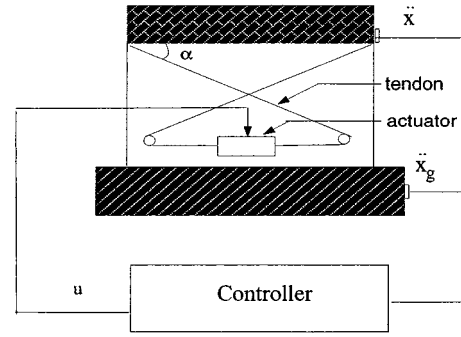


Fig. 2. Single-degree-of-freedom system with active tendon system

### Active Tendon System

The first example below analyzes a building modeled as a single-degree-of-freedom system. The second example analyzes a three-story building.

### Single-Degree-of-Freedom Building

The equation of motion of the SDOF system with tendons shown in Fig. 2 is given by

$$\ddot{x}_0(t) + 2\zeta\omega_0\dot{x}_0(t) + \omega_0^2 x_0(t) = -\ddot{x}_g(t) - \frac{4k_c \cos \alpha}{m} u_0(t) \quad (23)$$

where  $x_0$ ,  $\dot{x}_0$ , and  $\ddot{x}_0$  = horizontal relative displacement, velocity, and acceleration of the building floor;  $\ddot{x}_g$  = ground acceleration;  $u_0$  = actuator displacement;  $m$ ,  $\zeta$ , and  $\omega_0$  = mass, damping, and angular frequency, respectively;  $k_c$  = stiffness of the cable; and  $\alpha$  = cable angle. These parameters are defined as  $m = 2,922.7$  kg;  $\zeta = 0.0124$ ;  $\omega_0 = 21.79$  rad/s;  $k_c = 371,950.8$  N/m; and  $\alpha = 36^\circ$ . In this example,  $Q = I$ ,  $R = 460$ ,  $p = 5$ , and  $\lambda = 2$ .

Analysis of the SDOF system using MPC with acceleration feedback is compared to the analysis using MPC with state (i.e., displacement and velocity) feedback. In the former case, an observer is used to estimate the states of the system using the measured acceleration output. The estimator gain is obtained by the Kalman-Bucy filter as described in the section "Acceleration Feedback and State Estimator." The results are listed in Table 1. Using almost the same control force (the difference is 0.05% in RMS value and 1.22% in maximum value), these schemes give similar control performance. The transfer function for the acceleration feedback is shown in Fig. 3. The peak values of the system Bode plot show a significant increase in damping after the control force is included. The damping ratio with and without control was found to be 0.182 and 0.0124, respectively. Figs. 4 and 5 show the displacement and acceleration response of a building with and without control action, respectively. Fig. 6 shows the variation in control force for this control example.

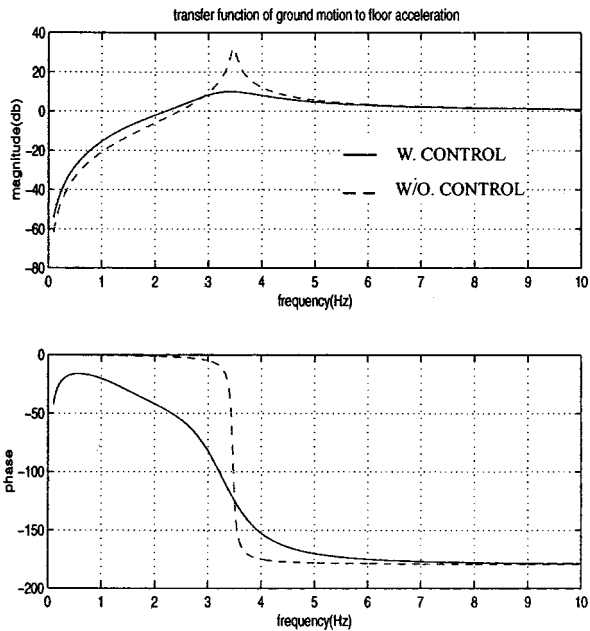
### Three-Story Building under Multivariable Control

In this example, a three-story building (Chung et al. 1989) is used to implement the MPC scheme using the acceleration feedback obtained from different locations. The mass, stiffness, and damping matrices of the building are given in Table 2. In this example, the stiffness of the active tendon is  $k_c = 3.7197 \times 10^5$  N/m and  $\alpha = 36^\circ$ . The active tendon is set up on the first floor (Fig. 7). In this example,  $Q = I$ ,  $R = 3,000$ ,  $p = 5$ , and  $\lambda = 2$ .

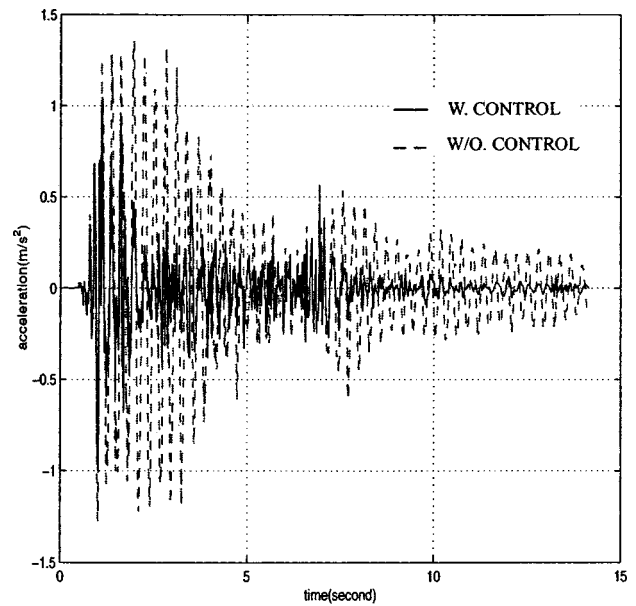
In the first case, the accelerometer is placed on each floor. The acceleration outputs are fed back to the observer, which estimates the states of the system. In the next three cases, the accelerometer

**Table 1.** Comparison between Model Predictive Control with State and with Acceleration Feedback

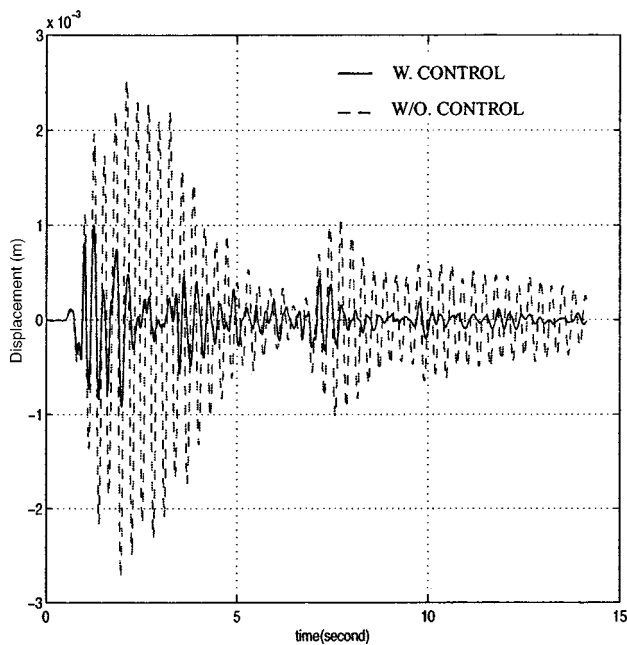
$p=5, \lambda=2$	Without control	Model predictive control with state feedback	Percentage change	Model predictive control with acceleration feedback	Percentage change
$\sigma_x$ (cm)	0.075	0.0201	73.34%	0.0202	73.16%
$\sigma_{\ddot{x}}$ (cm/s <sup>2</sup> )	37.79	14.64	61.26%	14.67	61.18%
$\sigma_f$ (N)	—	99.18	—	99.13	-0.05%
$x_{\max}$ (cm)	0.25	0.10	60.0%	0.10	60.0%
$\ddot{x}_{\max}$ (cm/s <sup>2</sup> )	135.36	101.52	25.00%	101.42	25.07%
$f_{\max}$ (N)	—	671.97	—	663.74	-1.22%



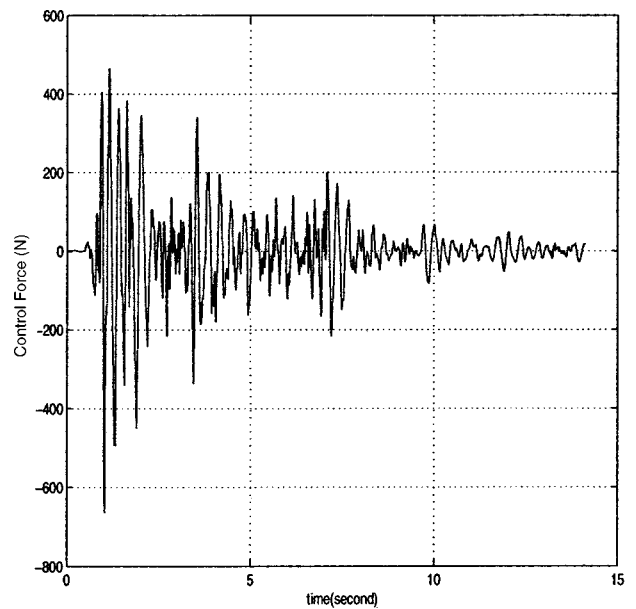
**Fig. 3.** Transfer function from ground acceleration to floor acceleration



**Fig. 5.** Comparison of uncontrolled and controlled acceleration with acceleration feedback



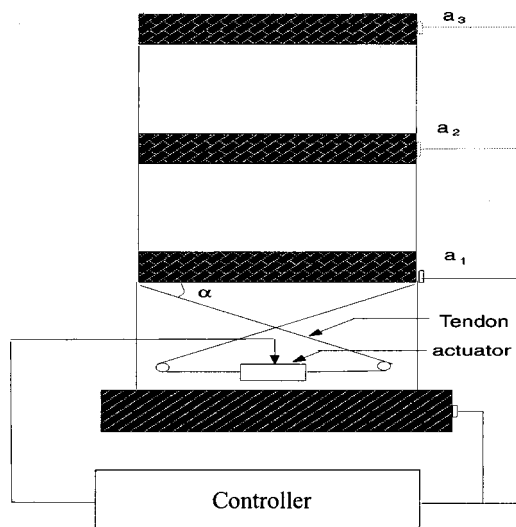
**Fig. 4.** Comparison of uncontrolled and controlled displacement with acceleration feedback



**Fig. 6.** Control force of model predictive control acceleration feedback

**Table 2.** Modeling Parameters for Three-Story Building

Parameter	Value
Mass matrix $\mathbf{M}$ (kg)	$\mathbf{M} = \begin{bmatrix} 974 & 0 & 0 \\ 0 & 974 & 0 \\ 0 & 0 & 974 \end{bmatrix}$
Stiffness matrix $\mathbf{K}$ (N/m)	$\mathbf{K} = \begin{bmatrix} 2.74 & -1.64 & 0.37 \\ -1.64 & 3.02 & -1.62 \\ 0.37 & -1.62 & 1.33 \end{bmatrix} \times 10^6$
Damping matrix $\mathbf{C}$ (N·s/m)	$\mathbf{C} = \begin{bmatrix} 382.65 & -57.27 & 61.64 \\ -57.27 & 456.73 & -2.63 \\ 61.64 & -2.63 & 437.29 \end{bmatrix}$

**Fig. 7.** Three-story building using active tendon control

is placed on one floor at a time. Therefore, only one acceleration output is known, which is used as an input into the observer to estimate the system states. The entire building responses using these four acceleration feedback configurations are compared in Table 3.

The RMS value of the control force remains unchanged in all four cases using different weighting matrices. There is a very small difference in the displacement response in all these cases. However, the difference in the acceleration response of these cases is large. Table 3 shows that the maximum control force is largest and the observed value of the RMS acceleration response is highest among all these cases if the accelerometer is placed on the third floor. If the accelerometer is placed only on the first floor, the RMS value of the acceleration response is smaller than in cases in which the accelerometer is placed on either the second or third floor. The acceleration response is most reduced if the acceleration feedback is obtained from all floor levels. This is because the acceleration feedback of all three floors contains more information about all three modes of the building and the active tendon can reduce all three modes of the structure. This makes results from the all-floor acceleration feedback most attractive, followed by the first-floor acceleration feedback.

For the all-floor acceleration feedback case, Fig. 8 gives the time history of the third-floor acceleration and Fig. 9 shows the control force generated by the active tendons.

In Figs. 10 and 11, the transfer functions from the ground motion to the first- and third-floor accelerations of the all-floor acceleration feedback case are shown. The three peaks occur at the first three natural frequencies of the structure, which represent the three modes. The dashed line represents the transfer functions of uncontrolled system. After the control action is included, the contributions of these modes are reduced as shown in the solid lines. All three modes are greatly reduced by the active tendon system.

### Active Mass Damper

The first example involving an AMD analyzes a building with a single degree of freedom, whereas the second example involves a three-story building equipped with an AMD.

**Table 3.** Comparison of Results Obtained using Various Accelerometer Layouts

	Uncontrolled	Three-floor feedback	First-floor feedback	Second-floor feedback	Third-floor feedback
$\sigma_{x1}$ (cm)	0.063	0.032	0.032	0.031	0.032
$\sigma_{x2}$ (cm)	0.126	0.067	0.067	0.066	0.067
$\sigma_{x3}$ (cm)	0.162	0.085	0.086	0.084	0.085
$\sigma_{\ddot{x}1}$ (cm/s <sup>2</sup> )	50.2	16.3	16.5	18.3	19.1
$\sigma_{\ddot{x}2}$ (cm/s <sup>2</sup> )	35.8	19.5	19.6	20.2	20.0
$\sigma_{\ddot{x}3}$ (cm/s <sup>2</sup> )	46.5	22.5	22.63	22.76	23.40
$\sigma_f$ (N)		51.60	51.60	51.60	51.60
$x_{1 \max}$ (cm)	0.185	0.109	0.113	0.112	0.110
$x_{2 \max}$ (cm)	0.310	0.225	0.233	0.225	0.228
$x_{3 \max}$ (cm)	0.380	0.288	0.299	0.287	0.288
$\ddot{x}_{1 \max}$ (cm/s <sup>2</sup> )	177.9	148.4	150.2	156.3	159.8
$\ddot{x}_{2 \max}$ (cm/s <sup>2</sup> )	134.1	103.2	103.2	113.5	110.5
$\ddot{x}_{3 \max}$ (cm/s <sup>2</sup> )	154.6	137.0	136.6	141.5	136.0
$f_{\max}$ (N)		173.37	175.37	170.34	190.97

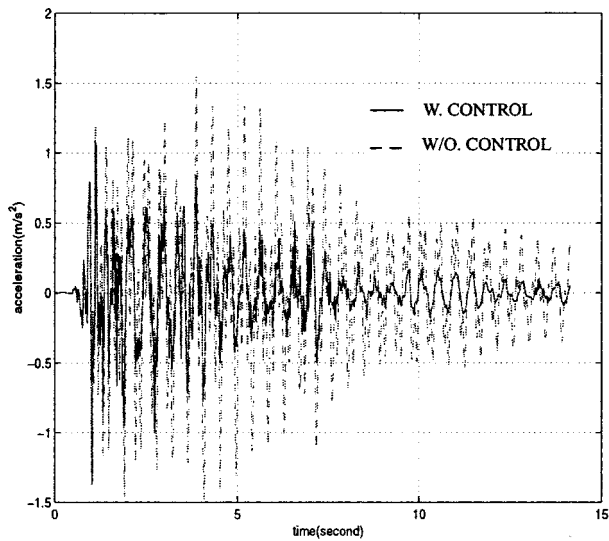


Fig. 8. Uncontrolled and controlled third-floor acceleration

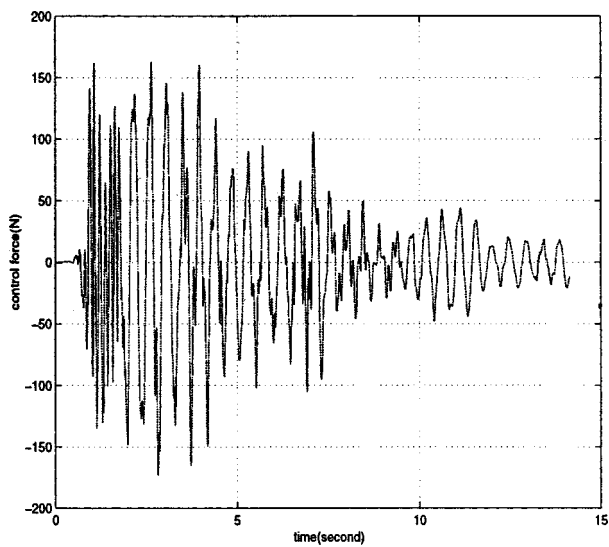


Fig. 9. Control force using active tendon

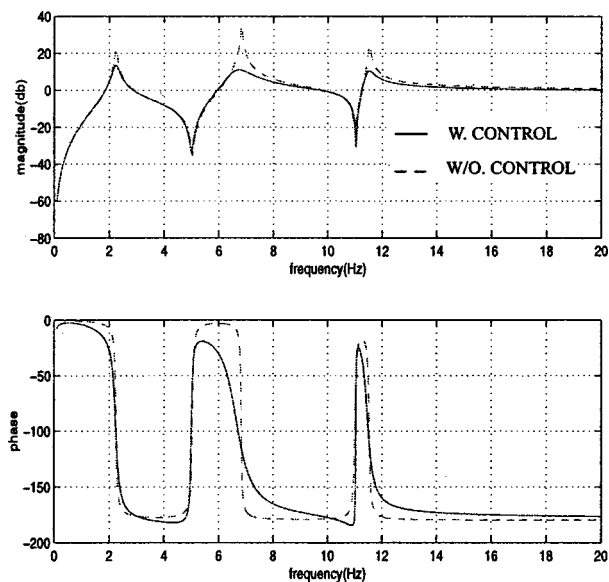


Fig. 10. Bode plot of ground motion to first-floor acceleration; all-floor feedback

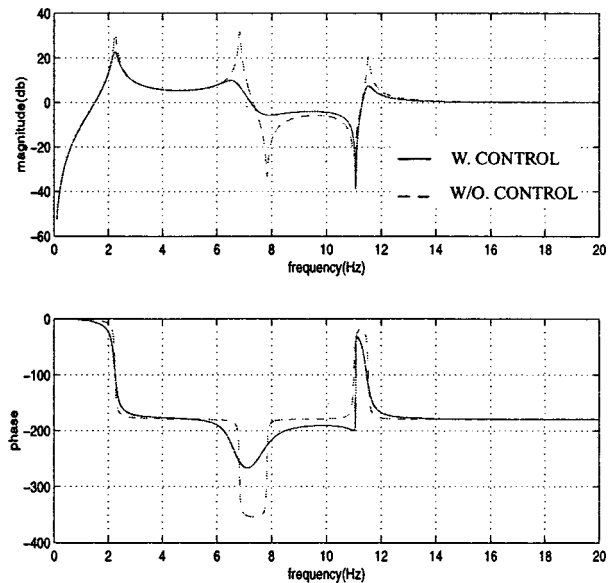


Fig. 11. Bode plot of ground motion to third-floor acceleration; all-floor feedback

### Single-Degree-of-Freedom System

In this example, the single-degree-of-freedom building is analyzed again using an active mass damper on the top of the building instead of the active tendon system (Fig. 12). The mass, damping ratio, and natural frequency of the AMD are, respectively,  $m_2=0.02m_1$ ,  $\zeta_2=0.1$ , and  $\omega_2=21.6$  rad/s. As before, MPC schemes using both state feedback and acceleration feedback are employed. The parameters are chosen as  $R=1$ ,  $Q = \text{diag}[500,000, 10, 0, 0]$ ,  $p=5$ , and  $\lambda=2$ . The results are shown in Table 4. Both the state and acceleration feedback schemes performed similarly. The maximum displacement and acceleration responses and RMS values of the displacement, acceleration, and control force were comparable. However, the maximum control force demanded by the acceleration feedback scheme was significantly larger than that of the state feedback scheme.

The transfer function relating the ground motion to building acceleration is plotted in Fig. 13. The response is greatly reduced around the structure's natural frequency. If the excitation frequency is far from the system natural frequency, the control system is least effective. There are two small peaks around 3.1 and

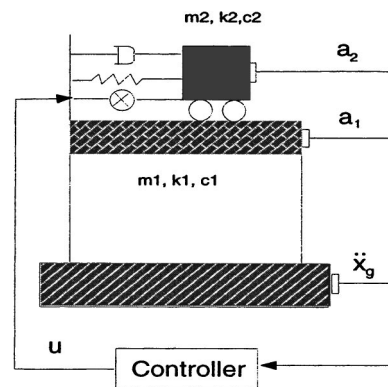
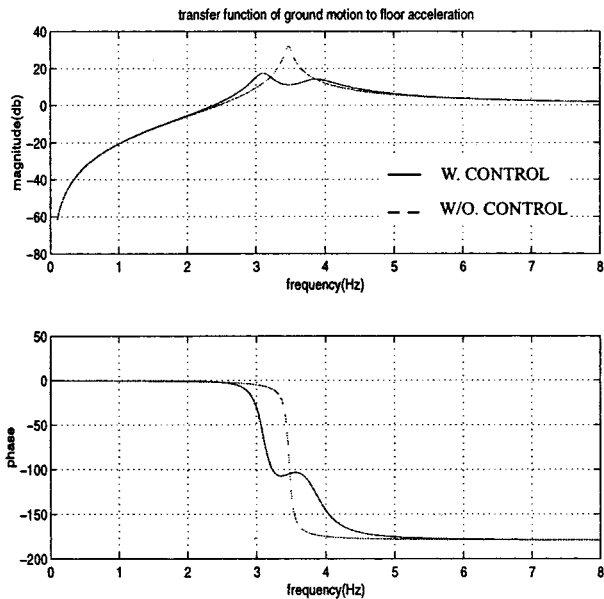


Fig. 12. Single-degree-of-freedom building using active mass damper

**Table 4.** Comparison between Model Predictive Control with State and with Acceleration Feedback Active Mass Damper

$p=5, \lambda=2$	Without control	Model predictive control with state feedback	Percentage change	Model predictive control with acceleration feedback	Percentage change
$\sigma_x$ (cm)	0.075	0.031	59.47	0.034	55.34
$\sigma_{\ddot{x}}$ (cm/s <sup>2</sup> )	37.79	19.95	47.21	20.57	45.57
$\sigma_u$ (N)	—	144.7	—	152.8	5.52
$x_{\max}$ (cm)	0.27	0.15	44.44	0.16	40.74
$\ddot{x}_{\max}$ (cm/s <sup>2</sup> )	135.36	126.45	6.58	126.68	6.41
$u_{\max}$ (N)	—	483.8	—	820.7	69.6



**Fig. 13.** Bode plot of ground motion to floor acceleration using active mass damper

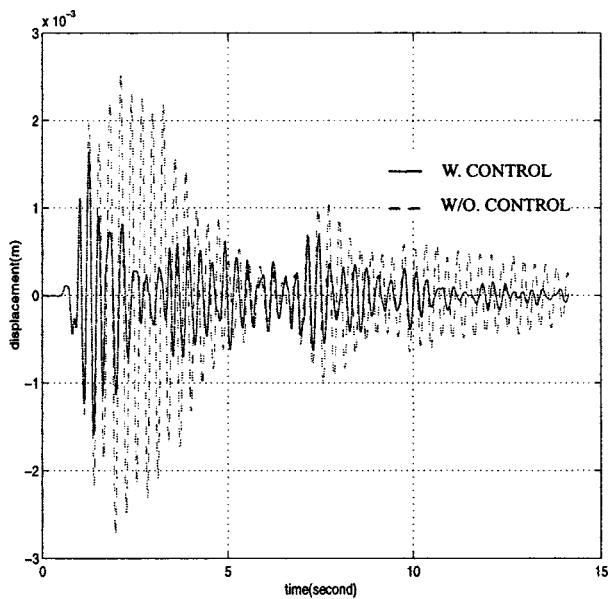


**Fig. 14.** Uncontrolled and controlled floor acceleration using active mass damper

3.8 Hz, which are due to the interaction between the AMD and the building. The damping ratio is increased from  $1.24 \times 10^{-2}$  (uncontrolled) to 0.176 (controlled). Therefore, the response of the system is reduced significantly. The time histories of the uncontrolled and controlled displacements of the building are shown in Fig. 14.

### Three-Story Building

The building analyzed previously is used again here with an active tuned mass damper placed on top of the third floor (Fig. 15). The natural frequency of the AMD is close to the first natural frequency of the building. The mass, damping ratio, and natural frequency of the AMD are, respectively,  $m_2 = 0.02m_1$ ,  $\zeta_2 = 0.2$ , and  $\omega_2 = 0.95\omega_1$  rad/s. Here,  $p=5$ ,  $\lambda=2$ ,  $Q = \text{diag}[10,000, 10,000, 50,000, 10, 0, 0, 0, 0]$ , and  $R=0.03$  are used.

In Table 5, the performance of the controller is reported for different configurations of the acceleration feedback as in the active tendon example. The control force is kept the same in all four cases by using different weighting matrices. In the four cases examined, the best control effects can be achieved if the acceleration is measured at the first floor. The all-floor feedback case provides a better performance than the second- or third-floor feedbacks.

Figs. 16 and 17 show the transfer functions from the ground motion to the top-floor acceleration of the all-floor feedback case. It is noted that the first-mode contribution is reduced significantly, followed by the second, and with no noticeable change in the

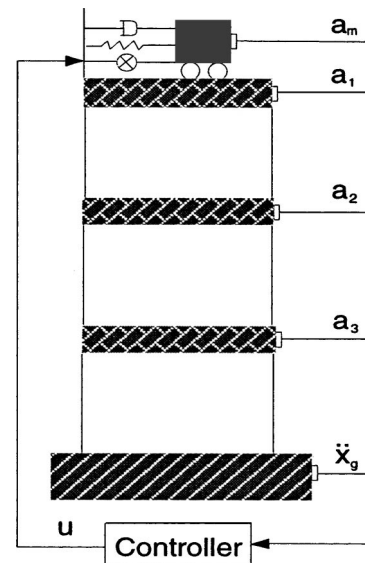


**Fig. 15.** Three-story building using active mass damper

**Table 5.** Comparison of Results Obtained using Various Accelerometer Layouts

	Uncontrolled	Three-floor feedback	First-floor feedback	Second-floor feedback	Third-floor feedback
$\sigma_{x1}$ (cm)	0.063	0.023	0.021	0.023	0.024
$\sigma_{x2}$ (cm)	0.126	0.038	0.039	0.039	0.039
$\sigma_{x3}$ (cm)	0.162	0.049	0.050	0.050	0.051
$\sigma_{\ddot{x}1}$ (cm/s <sup>2</sup> )	50.2	32.54	25.61	30.63	34.34
$\sigma_{\ddot{x}2}$ (cm/s <sup>2</sup> )	35.78	21.98	21.04	21.89	22.58
$\sigma_{\ddot{x}3}$ (cm/s <sup>2</sup> )	46.5	24.33	20.96	23.49	25.50
$\sigma_f$ (N)		32.56	32.56	32.56	32.56
$x_{1 \max}$ (cm)	0.185	0.131	0.130	0.134	0.139
$x_{2 \max}$ (cm)	0.310	0.217	0.224	0.224	0.225
$x_{3 \max}$ (cm)	0.380	0.286	0.267	0.274	0.284
$\ddot{x}_{1 \max}$ (cm/s <sup>2</sup> )	177.9	164.1	155.4	161.5	167.1
$\ddot{x}_{2 \max}$ (cm/s <sup>2</sup> )	134.1	137.0	120.3	134.6	138.0
$\ddot{x}_{3 \max}$ (cm/s <sup>2</sup> )	154.6	136.1	133.0	138.8	140.6
$f_{\max}$ (N)		180.2	186.3	184.4	181.4

third mode. For the first-floor case, all three modes are in the same phase. The first-floor acceleration feedback can provide a better estimate of the states of the system and AMD, therefore, reduces the first mode significantly. Accordingly, the first-floor acceleration feedback results in reducing the acceleration response more effectively.

### Experimental Validation

To verify the effectiveness of acceleration feedback based on the MPC scheme, experiments were conducted at the NatHaz Modeling Laboratory, University of Notre Dame. Accelerometers were used to measure the acceleration feedback and for designing the observer to evaluate the system states. The test equipment included a small-scale shaking table device, a steel column building

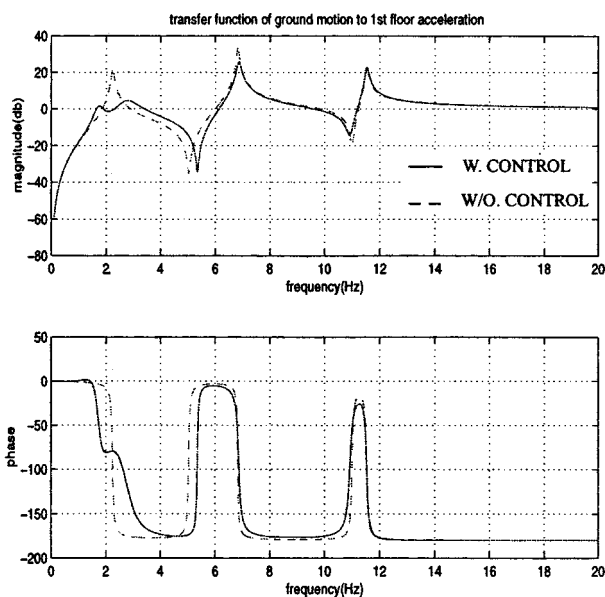


**Fig. 16.** Bode plot of ground motion to first-floor acceleration; all-floor feedback using active mass damper

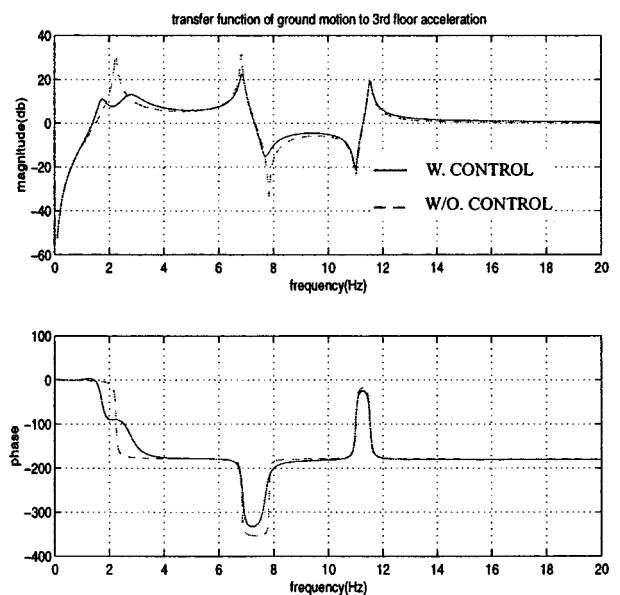


**Fig. 17.** Bode plot of ground motion to third-floor acceleration; all-floor feedback using active mass damper

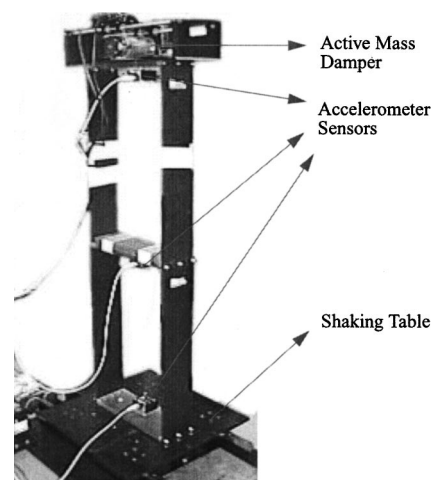


**Fig. 18.** Experimental building and active mass damper on shaking table with accelerometers

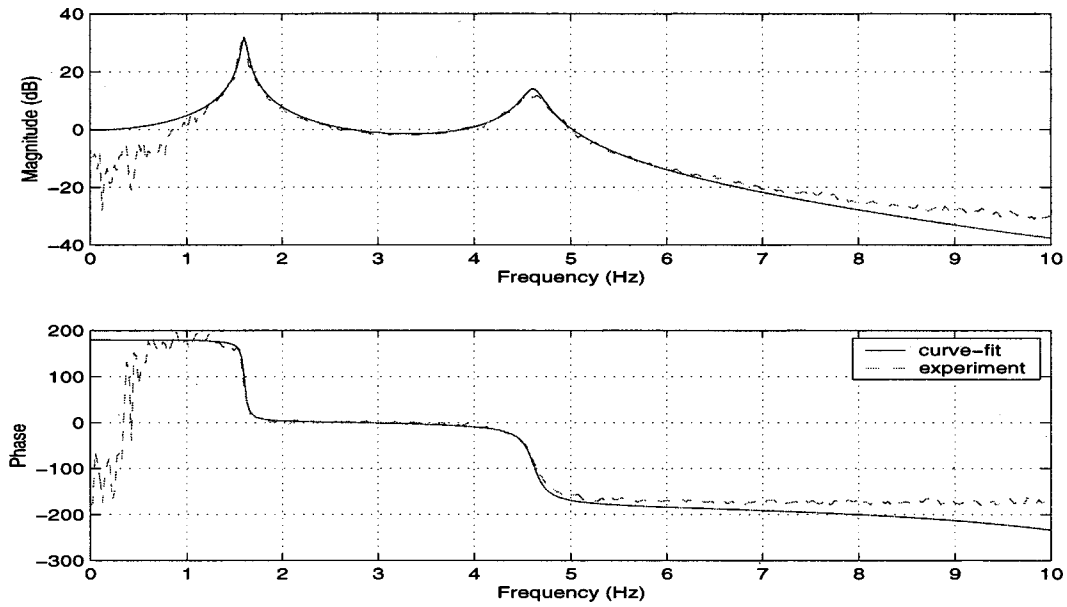


Fig. 19. Transfer function from ground acceleration to second-floor acceleration

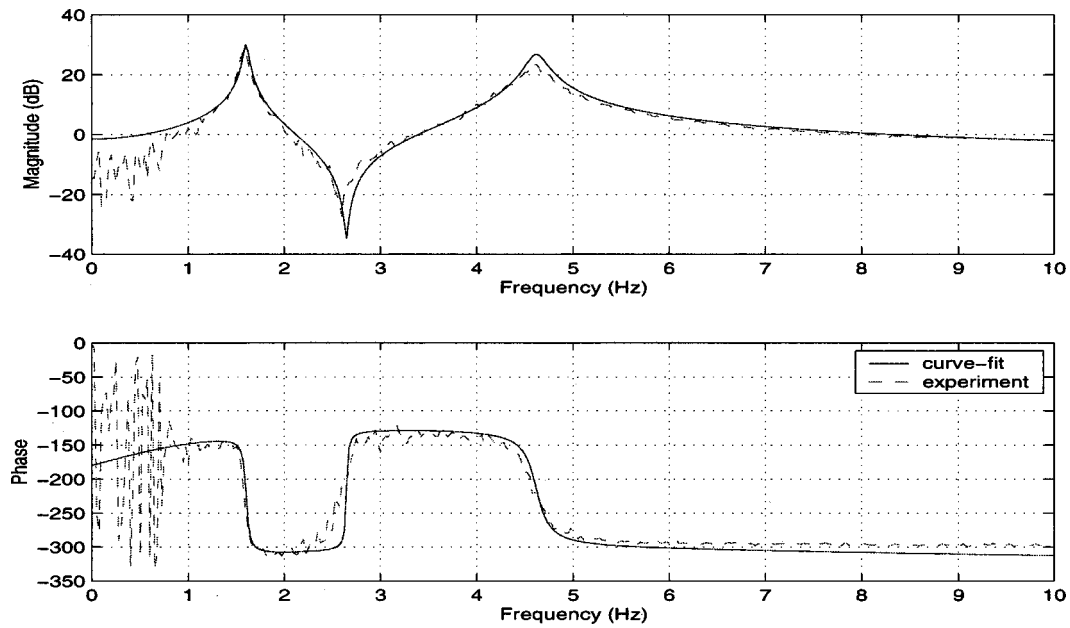


Fig. 20. Transfer function from ground acceleration to first-floor acceleration

Table 6. Experimental Results

	$\sigma_{\ddot{x}_{a2}}$ (cm/s <sup>2</sup> )	$\sigma_{\ddot{x}_{a1}}$ (cm/s <sup>2</sup> )	$\sigma_u$ (mV)	$\max( \ddot{x}_{a2} )$ (cm/s <sup>2</sup> )	$\max( \ddot{x}_{a1} )$ (cm/s <sup>2</sup> )	$\max( u )$ (mV)
Uncontrolled	42.93	37.84		139.7	121.10	
Controlled (experiment)	24.09	21.91	52.0	93.08	95.24	219.5
Controlled (simulation)	22.15 (8.1%)	18.59 (15.2%)	47.2 (9.2%)	90.56 (2.7%)	88.01 (7.6%)	209.0 (4.8%)

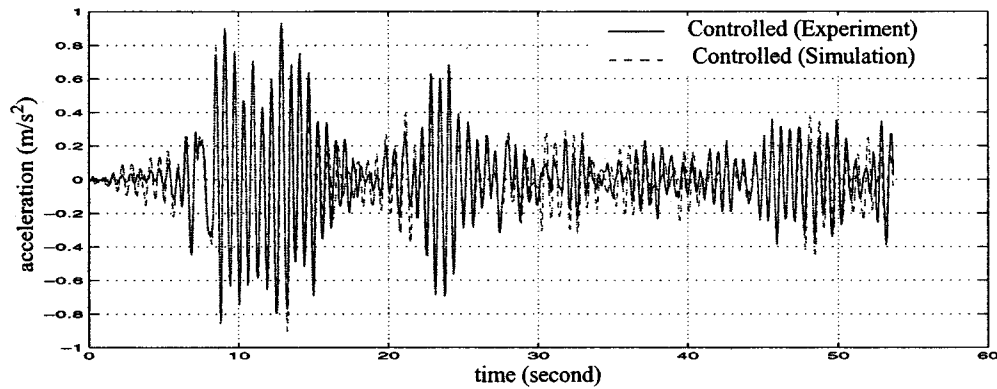


Fig. 21. Time history of second-floor acceleration using the model predictive control scheme (solid line, experiment; dashed line, simulation)

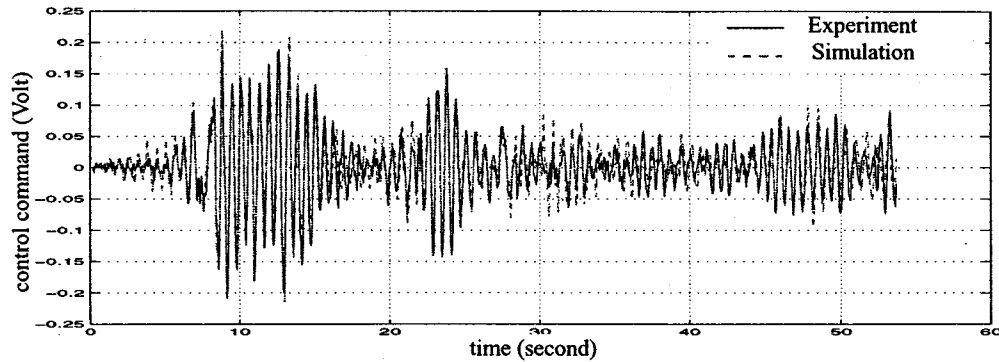


Fig. 22. Time history of control command to active mass damper using the model predictive control scheme (solid line, experiment; dashed line, simulation)

model, an active mass damper, a multichannel data acquisition I/O board, a signal spectrum analyzer, accelerometers, and a computer.

The small-scale shaking table consists of an electric powered servomotor, a 46 cm×46 cm flat table mounted on one linear high-accuracy driving shaft, and two 64-cm-long sliding tracks. The two-story test building employed in the experiment and shown in Fig. 18 is a flexible scale model. This structure is configured to have two floors. The height of each floor was 490 mm with two steel columns with dimensions of 2×108×490 mm<sup>3</sup>. The mass of each column was 0.227 kg. The first-floor mass was 4.8 kg. The mass of the second floor including AMD was 5.0 kg; the AMD was a direct-drive linear motion cart driven by a high-torque DC motor. Accelerometers were attached at each floor. A multi-I/O board was used for data acquisition. It was used to obtain the measured response from sensors and to send control signals to the shaking table and AMD.

The system was identified by curve fitting and an eigenvalue realization algorithm (ERA). The first step to get the analytical state space representation of the system from the experimentally obtained transfer function involves curve fitting. The Matlab function *invfreq* is used to curve-fit each individual term of the transfer function matrix  $H(s)$ . Once curve fitting is completed, the left matrix-fraction method is used to obtain the Markov parameters, which are used as the basis for identifying mathematical models for linear dynamic systems using ERA identification (Juang 1994).

The dynamics of the AMD and the interaction between the AMD and the building were included in the system identification.

Five poles including two pairs of complex poles and one real pole were identified for the entire system. Fig. 19 shows the transfer function from the ground acceleration to the second-floor acceleration. Fig. 20 shows the transfer function from the ground acceleration to the first-floor acceleration. The results show good agreement between the building model and the experimental data.

The RMS and peak values of the acceleration response and the control command voltage are listed in Table 6. The MPC scheme greatly reduced the acceleration response of the two-story building. Fig. 21 shows a comparison between the experimental and simulated time histories of the second-floor acceleration controlled by the MPC scheme using the acceleration feedback. Fig. 22 shows a comparison between the experimental and simulated results of the control command sent to the AMD using the MPC scheme. There is only a small difference between the experimental and simulation response values.

## Conclusion

In this paper, a MPC-based scheme using the acceleration response feedback was presented for controlling structural response to earthquake-induced motions. An observer employing the Kalman-Bucy filter was utilized to estimate the states of the system from the measured acceleration output. The performances of a single-story and a three-story building equipped with an active tendon and AMD systems were analyzed. In these examples, the MPC scheme that utilized the acceleration feedback was compared to the MPC scheme with state feedback. The results suggest

that the acceleration feedback scheme produced either an equivalent or better performance. Furthermore, the acceleration feedback from different floors resulted in different control performance for active tendon and AMD controlled buildings. Experimental validation of the control scheme was provided to demonstrate MPC's effectiveness in digital implementation.

This paper demonstrated, by way of numerical and experimental examples, the effectiveness of the MPC scheme in controlling structural motions under earthquakes. It is envisaged that such studies will promote examination and implementation of this versatile scheme, noted for its computational expediency, natural extension to real-time applications, intrinsic convenience in the treatment of constraints, and potential for future applications.

## Acknowledgments

Support for this work was provided in part by the National Science Foundation Grant Nos. CMS-94-02196 and CMS-95-03779 under the NSF Structure Control Initiative. This support is gratefully acknowledged.

## References

- Camacho, E. F., and Bordons, C. (1999). *Model predictive control*, Springer-Verlag, London.
- Chung, L. L., Lin, R. C., Soong, T. T., and Reinhorn, A. M. (1989). "Experimental study of active control for MDOF seismic structures." *J. Eng. Mech.*, 115(8), 1609–1627.
- Doyle, J. C., Glover, K., Khargonekar, P., and Francis, B. (1989). "State-space solutions to standard  $H_2$  and  $H_\infty$  control problems." *IEEE Trans. Autom. Control*, 34, 831–847.
- Dyke, S. J., Spencer, B. F., Quast, P., Sain, M. K., Kaspari, D. C., and Soong, T. T. (1996). "Acceleration feedback control of MDOF structures." *J. Eng. Mech.*, 122(9), 907–917.
- Garcia, C. E., and Morari, M. (1982). "Internal model control. 1. A unifying review and some new results." *Ind. Eng. Chem. Process Des. Dev.*, 21, 308–323.
- Housner, G. W., Bergman, L. A., Caughey, T. K., Chassiakos, A. G., Claus, R. O., Masri, S. F., Skelton, R. E., Soong, T. T., Spencer, B. F., and Yao, J. T. P. (1997). "Structural control: Past, present, and future." *J. Eng. Mech.*, 123(9), 897–971.
- Juang, J. N. (1994). *Applied system identification*, Prentice-Hall, Englewood Cliffs, N.J.
- Kailath, T. (1980). *Linear systems*, Prentice-Hall, Englewood Cliffs, N.J.
- Kareem, A., Kijewski, T., and Tamura, Y. (1999). "Mitigation of motions of tall buildings with specific examples of recent applications." *Wind Struct.*, 2(3), 201–251.
- Kwon, W. H., and Byun, D. G. (1989). "Receding horizon tracking control as a predictive control and its stability properties." *Int. J. Control*, 50(5), 1807–1824.
- Lopez-Almansa, F., Andrade, R., Rodellar, J., and Reinhorn, A. M. (1994a). "Modal predictive control of structures I: Formulation." *J. Eng. Mech.*, 120(8), 1743–1760.
- Lopez-Almansa, F., Andrade, R., Rodellar, J., and Reinhorn, A. M. (1994b). "Modal predictive control of structures II: Implementation." *J. Eng. Mech.*, 120(8), 1761–1772.
- Mei, G., Kareem, A., and Kantor, J. C. (1998). "Real-time model predictive control of structures under earthquakes." *Proc., 2nd World Conf. on Structural Control*, Kyoto, Japan, 1585–1594.
- Mei, G., Kareem, A., and Kantor, J. C. (2000). "Model predictive control for wind excited buildings: A benchmark problem." *Proc., 14th Engineering Mechanics Conf.*, ASCE, New York.
- Mei, G., Kareem, A., and Kantor, J. C. (2001). "Real-time model predictive control of structures under earthquakes." *Earthquake Eng. Struct. Dyn.*, 30, 995–1019.
- Morari, M., Garcia, C. E., Lee, D. M., and Pretz, D. M. (1994). *Model predictive control*, Prentice-Hall, Englewood Cliffs, N.J.
- Morari, M., and Lee, J. H. (1991). "Model predictive control: The good, the bad, and the ugly." *Proc., 4th Int. Conf. on Chemical Process Control*, AIChE, Padre Island, Tex., 17–22.
- Qin, S. J., and Badgwell, T. J. (1996). "An overview of industrial model predictive control technology." *Proc., Chemical Process Control-V*, AIChE Symposium Series 316, Vol. 93, CACHE and American Institute of Chemical Engineers, New York, 232–256.
- Ricker, L. (1990). "Model predictive control with state estimation." *Ind. Eng. Chem. Res.*, 29, 374–382.
- Rodellar, J., Barbat, A. H., and Matin-Sanchez, J. M. (1987). "Predictive control of structures." *J. Eng. Mech.*, 113(6), 797–812.
- Slotine, J. J. E. (1984). "Sliding controller design for nonlinear systems." *Int. J. Control*, 40(2), 421–434.
- Soong, T. T. (1990). *Active structural control: Theory and practice*, Longman Scientific and Technical, Essex, England.
- Soong, T. T., and Dargush, G. F. (1997). *Passive energy dissipation systems in structural engineering*, Wiley, New York.
- Spencer, B. F., Jr., Suhardjo, J., and Sain, M. K. (1994). "Frequency domain optimal control strategies for aseismic protection." *J. Eng. Mech.*, 120(1), 135–158.
- Suhardjo, J., and Kareem, A. (1997). "Structural control of offshore platforms." *Proc., 7th Int. Offshore and Polar Engineering Conf. ISOPE-97*, Honolulu.
- Suhardjo, J., Spencer, B. F., Jr., and Kareem, A. (1992). "Frequency domain optimal control of wind-excited buildings." *J. Eng. Mech.*, 118(12), 2463–2481.
- Utkin, V. I. (1977). "Variable structure systems with sliding modes." *IEEE Trans. Autom. Control*, AC-22, 212–222.
- Yang, J. N., Wu, J. C., Reinhorn, A. M., Riley, M., Schmitendorf, W. E., and Jabbari, F. (1994). "Experimental verifications of  $H_\infty$  and sliding mode control for seismic-excited buildings." *Proc., 1st World Conf. on Structure Control*, Pasadena, Calif., 63–72.
- Zafriou, E. (1991). "On the effect of tuning parameters and constraints on the robustness of model predictive controllers." *Proc., 4th Int. Conf. on Chemical Process Control*, AIChE, Padre Island, Tex.